Geophysical Research Letters

RESEARCH LETTER
10.1029/2023GL106359

Modeling the Effects of Drift Orbit Bifurcation on the Magnetopause Shadowing Loss of Radiation Belt Electrons

Jinbei Huang[1], Xingzhi Lyu[1], Weichao Tu[1], Jay M. Albert[2], and Sang-Yun Lee[1]

[1]Department of Physics and Astronomy, West Virginia University, Morgantown, WV, USA, [2]Air Force Research Laboratory, Kirtland AFB, Albuquerque, NM, USA

Key Points:

- A radial diffusion model with event-specific last closed drift shell (LCDS) is used to simulate the electron magnetopause shadowing loss
- Different approaches to dealing with the drift orbit bifurcation (DOB) effects are implemented in the calculation of LCDS
- The model best reproduces the observations when LCDS is calculated by tracing test particles and physically including DOB

Correspondence to:
J. Huang,
jh0049@mix.wvu.edu

Citation:
Huang, J., Lyu, X., Tu, W., Albert, J. M., & Lee, S.-Y. (2023). Modeling the effects of drift orbit bifurcation on the magnetopause shadowing loss of radiation belt electrons. *Geophysical Research Letters*, *50*, e2023GL106359. https://doi.org/10.1029/2023GL106359

Received 13 SEP 2023
Accepted 4 DEC 2023

Abstract Last closed drift shell (LCDS) has been identified as a crucial parameter for investigating the magnetopause shadowing loss of radiation belt electrons. However, drift orbit bifurcation (DOB) effects have not been physically incorporated into the LCDS calculation. Here we calculate event-specific LCDS using different approaches to dealing with the DOB effects, that is, tracing field lines ignoring DOB, tracing test particles rejecting field lines with DOB, and tracing particles including field lines with DOB, and then incorporate them into a radial diffusion model to simulate the fast electron dropout observed by Van Allen Probes in May 2017. The model effectively captures the fast dropout at high L^* and exhibits the best agreement with data when LCDS is calculated by tracing test particles with DOB more physically included. This study represents the first quantitative modeling of the DOB effects on radiation belt magnetopause shadowing loss via a more physical specification of LCDS.

Plain Language Summary Magnetopause shadowing has been recognized as a significant loss mechanism contributing to the rapid dropouts of radiation belt electrons. The last closed drift shell (LCDS), a critical input in modeling the magnetopause shadowing loss, is typically calculated by tracing magnetic field lines with constant second adiabatic invariant and magnetic field strength at particle's mirror point (B_m). However, the effects of drift orbit bifurcation (DOB) have not been realistically incorporated into the LCDS estimation for dropout modeling. DOB occurs when the local maximum of the magnetic field strength on the equator exceeds B_m, causing particles to be trapped in one hemisphere and leading to the violation of the second adiabatic invariant. To evaluate the effects of DOB on shadowing loss, we implemented three different LCDS calculations, that is, tracing field lines ignoring DOB, tracing test particles rejecting field lines with DOB, and tracing test particles including field lines with DOB, in a one-dimensional radial diffusion model. By reproducing the electron dropout observed at high L^* during the geomagnetic storm in May 2017, we discovered, for the first time, that physically incorporating DOB effects into the LCDS calculation via test particle tracing can best capture the observed electron loss at high L^*.

1. Introduction

Studies on Earth's radiation belts are becoming increasingly important since energetic particles trapped in the belts (Van Allen et al., 1958, 1959) can damage the electronic systems in space (Baker et al., 2018). Observations have shown that the MeV radiation belt electron flux can drop by several orders of magnitude within a few hours, which are called radiation belt dropouts (Shprits et al., 2016; Tu et al., 2009, 2010, 2014; Turner et al., 2012, 2014; Xiang et al., 2017, 2018). Many studies on electron dropouts have suggested two main loss mechanisms for MeV radiation belt electrons: magnetopause shadowing associated with outward radial diffusion (e.g., Katsavrias et al., 2019; Shprits et al., 2006, 2012; Turner et al., 2012, 2014; Ukhorskiy et al., 2006; Xiang et al., 2017), and precipitation into the atmosphere through the interaction with electromagnetic ion cyclotron (EMIC) waves (Blum et al., 2015; Capannolo et al., 2019; Lyu et al., 2022; Shprits et al., 2016; Zhang et al., 2016).

Magnetopause shadowing, the focus of this work, is modeled and evaluated for radiation belt electron dropout using the last closed drift shell (LCDS) (George et al., 2022; Olifer et al., 2018, 2021; Tu et al., 2014, 2019; Wang & Shprits, 2019; Wang et al., 2020; Xiang et al., 2017; Yu et al., 2013). LCDS is defined as the largest Roederer L^* (Roederer & Zhang, 2014) for drift shells that do not intersect with the magnetopause or open field lines. This is suggested as being more realistic than the magnetopause standoff distance in units of Earth radii (R_E) from Shue et al. (1998) model (hereafter referred to as rShue) when assessing the magnetopause shadowing losses (Olifer et al., 2018). However, Drift Orbit Bifurcation (DOB), violating the second adiabatic invariant

K, should be carefully considered in the estimation of LCDS (George et al., 2022; Olifer et al., 2018, 2021; Tu et al., 2014, 2019; Xiang et al., 2017; Yu et al., 2013). DOB occurs when the dayside magnetosphere is compressed by the solar wind, resulting in a W-shaped magnetic field strength profile with two minima off the magnetic equator and a maximum at the equator. A particle bouncing between two hemispheres becomes trapped on one hemisphere if it crosses the W-shaped field strength region with its B_m (the magnetic field intensity at the particle's mirror points) smaller than the equatorial magnetic field maximum (Huang et al., 2022; Öztürk & Wolf, 2007; Ukhorskiy et al., 2011). DOB violates both second and third adiabatic invariants of electrons, and the third invariant L^* becomes undefined. Therefore, the traditional method of obtaining LCDS by tracing magnetic field lines with constant second invariant (hereafter referred to as TF) cannot physically include DOB. To test the DOB effects in the LCDS calculation, Albert et al. (2018) utilized a guiding center test particle code to compute the LCDS through two approaches to addressing DOB: rejecting and including field lines with DOB (hereafter referred to as TPR and TPI, respectively). The former TPR approach assumes that electrons with a bifurcated drift shell are all lost within one drift, which could lead to an overestimation of the electron loss since results show that electrons can remain trapped in the radiation belt after the transport due to DOB (e.g., Huang et al., 2022). In the latter TPI approach of including field lines with DOB, the test particle code continues to trace the full drift trajectory of electrons after bifurcation and a pseudo-L^* is calculated based on the magnetic flux enclosed by the drift shell (even though it is not closed). Then Albert et al. (2018) compared the LCDS values calculated from these two approaches with the LCDS calculated using the traditional TF approach, and suggested that the LCDS calculated by these three different approaches can be very different during geomagnetic storms.

Even though previous work has shown that DOB can have significant effects on the electron LCDS, its effects on the dropout of radiation belt electrons have not been quantified. In this paper, for the first time, we implement the event-specific LCDS calculated using three different approaches to dealing with DOB, that is, tracing field lines ignoring DOB, tracing test particles rejecting field lines with DOB, and tracing test particles including field lines with DOB, into a radial diffusion model, to quantify the DOB effects on the observed magnetopause shadowing loss of radiation belt electrons during the May 2017 dropout event.

2. Event Analysis

The event we studied is an intense geomagnetic storm during May 27–28, 2017 with SYM-H reaching ∼−150 nT as shown in Figure 1e (black line for SYM-H, blue for Kp). The solar wind dynamic pressure P_{dyn} and the interplanetary magnetic field (IMF) B_z during the event are plotted in Figure 1d. Figures 1a and 1b plot the Phase Space Density (PSD) of the electrons with first and second invariants of $\mu = 912$ MeV/G and $K = 0.11$ $G^{1/2}R_E$ (corresponding to ∼2.2 MeV electrons at $L \sim 5$), $\mu = 2290$ MeV/G and $K = 0.11$ $G^{1/2}R_E$ (corresponding to ∼5.5 MeV electrons at $L \sim 5$) respectively, as a function of time and L^*. The PSD is calculated based on the flux measurements from the Relativistic Electron Proton Telescope (REPT) (Baker et al., 2013) and the Magnetic Electron Ion Spectrometer (MagEIS) instruments (Blake et al., 2013) onboard Van Allen Probes, using the TS04 magnetic field model (Tsyganenko & Sitnov, 2005). The PSD observations show some initial electron loss starting near the end of May 27 at $L^* \sim 4.5$–5. Then more significant dropout in PSD was observed at high L^* regions around 03 UT of May 28 for a wide range of μ values, which indicates loss of electrons through magnetopause shadowing. Figure 1c illustrates the 2.1 MeV electron fluxes as a function of local pitch angle and time, observed by Van Allen Probe A along its orbit. The observed fluxes at approximately 23 UT of May 27 near the apogee exhibit a distinct butterfly pitch angle distribution (PAD), which is a typical feature of the magnetopause shadowing loss due to drift shell splitting effect (Roederer & Zhang, 2014; Tu et al., 2019). The observed loss features discussed above suggest that magnetopause shadowing loss could be the dominant loss mechanism contributing to the dropout of outer radiation belt electrons during the 27 May 2017 storm, especially at high L^* regions.

3. Simulation and Results

3.1. Radial Diffusion Simulation

To simulate the magnetopause shadowing loss associated with the outward radial diffusion of electrons during the May 2017 dropout event, we employ a one-dimensional radial diffusion model that solves the Fokker-Planck equation (Schulz & Lanzerotti, 1974):

$$\frac{\partial f}{\partial t} = L^{*2}\frac{\partial}{\partial L^*}\left(\frac{D_{LL}}{L^{*2}}\frac{\partial f}{\partial L^*}\right) - \frac{f}{\tau}. \quad (1)$$

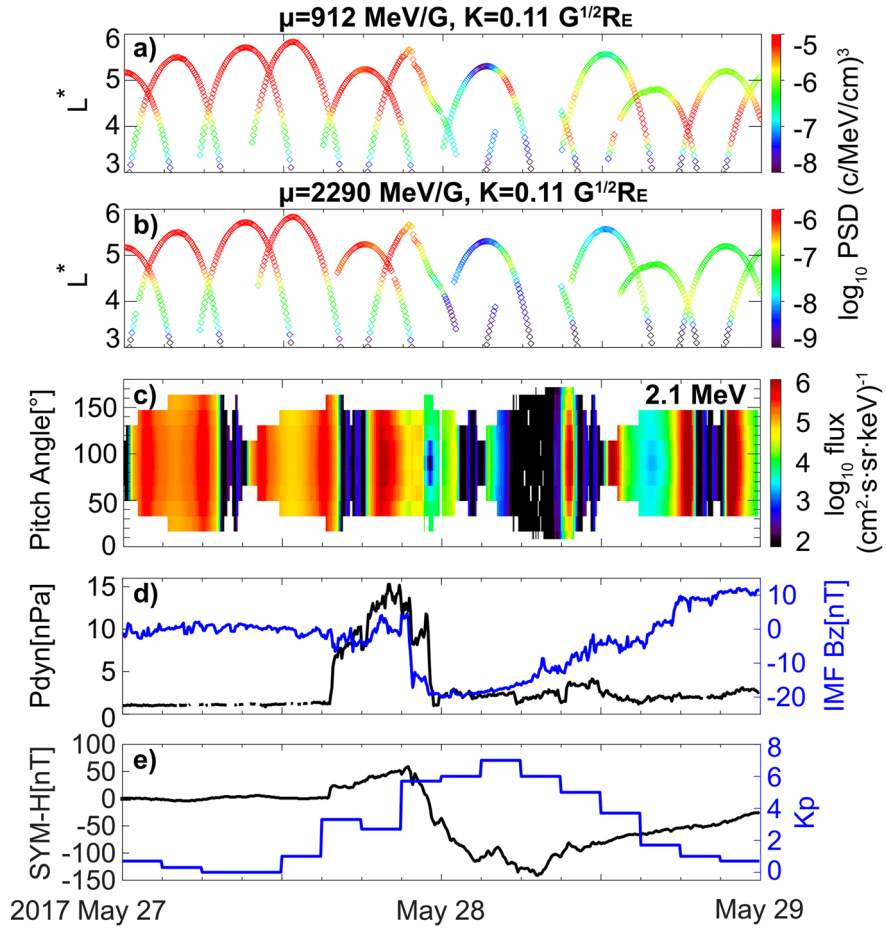

Figure 1. PSD of (a) μ = 912 MeV/G, (b) μ = 2290 MeV/G, and K = 0.11 $G^{1/2}R_E$ electrons as a function of time and L^*. (c) 2.1 MeV electron fluxes versus local pitch angle and time observed by Van Allen Probe A along its orbit. (d) Solar wind P_{dyn} in black, IMF B_z in blue, and (e) SYM-H (black line) and Kp (blue line) indices during May 27–28, 2017.

Here, f represents the electron PSD at a fixed μ and K. D_{LL} denotes the radial diffusion coefficient, and τ stands for the electron e-folding lifetime. The D_{LL} is obtained from the empirical radial diffusion coefficient from Brautigam and Albert (2000), which was derived up to Kp = 6 and for equatorially mirroring electrons. Here it is also applied to Kp > 6 intervals and to electrons at all pitch angles due to the unresolved pitch angle dependence of D_{LL} (e.g., Li et al., 2016; Miyoshi et al., 2006; Sarris et al., 2022). To represent the magnetopause shadowing loss, electron lifetimes outside the LCDS are assumed to be on the order of electron drift periods. The model outer boundary, a Neumann boundary condition ($\partial f/\partial L^* = 0$) defined at $L^* = 11$, remains outside the LCDS during this event.

The event-specific LCDS, calculated using the TS04 magnetic field model, employs three approaches to addressing DOB effects following Albert et al. (2018) (discussed in Section 1). The results are shown in Figure 2a1 for K = 0.05 $G^{1/2}R_E$. The first approach is the traditional approach by tracing magnetic field lines with constant second invariant using the International Radiation Belt Environment Modeling (IRBEM) library (Boscher et al., 2022). The calculated LCDS has a time resolution of 5 min and is depicted as the green line in Figure 2a1 and labeled as LCDS(TF), which is not physical when DOB occurs since DOB violates the second invariant. The remaining approaches utilize the guiding center test particle code, solving the guiding center equations by Brizard and Chan (1999).

In the second approach, tracing test particles while rejecting field lines with DOB, electrons with a bifurcated drift shell are assumed to be lost within one drift. This approach could be an "overkill" since electrons suffering from DOB may still be trapped in the radiation belt. This LCDS is shown as the orange line in Figure 2a1, labeled LCDS(TPR). The third approach, including field lines with DOB, calculates the magnetic flux enclosed by the bifurcated drift shells, creating a pseudo-L^* in the presence of DOB (Albert et al., 2018; Ukhorskiy et al., 2014).

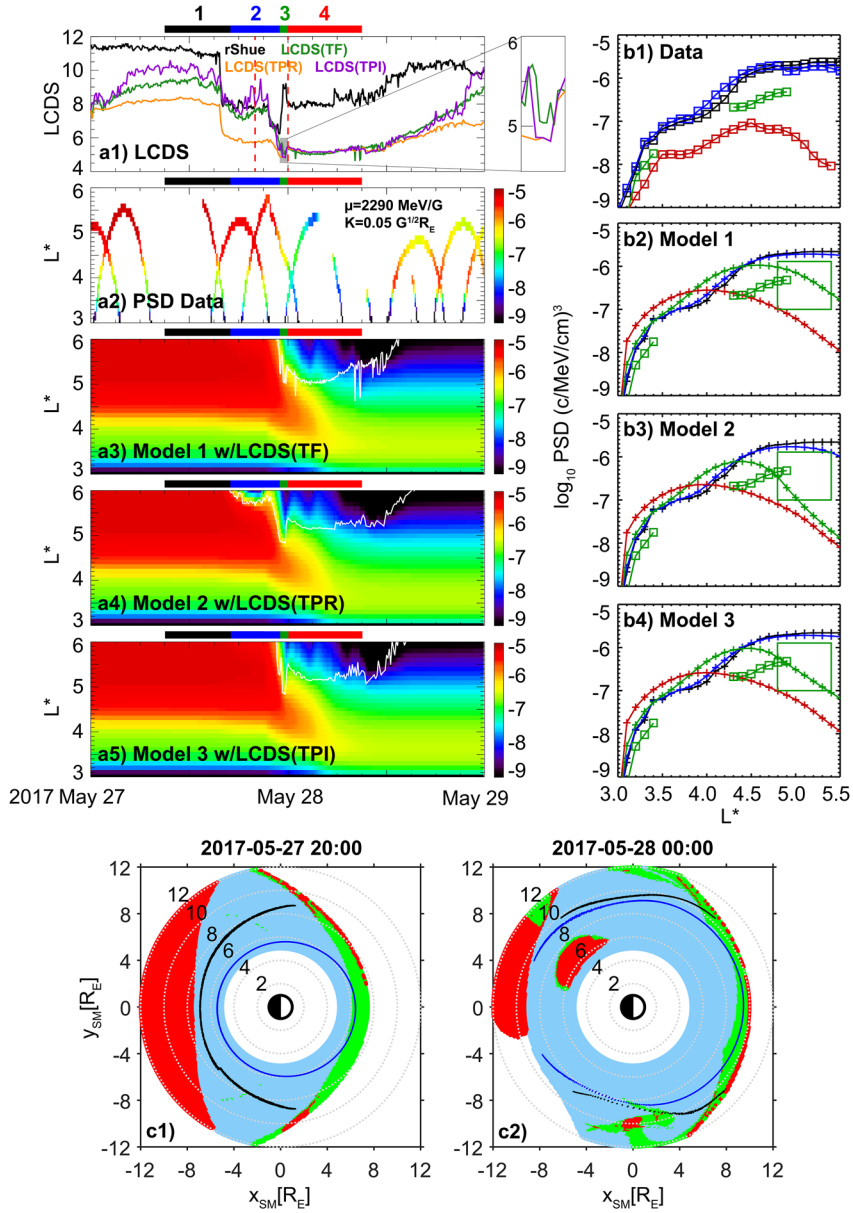

Figure 2. (a1) Different LCDS results of $K = 0.05\ G^{1/2}R_E$ electrons as a function of time. (a2–a5) Electron PSD data and simulation results for $\mu = 2290$ MeV/G, and $K = 0.05\ G^{1/2}R_E$, with the white curves in (a3–a5) representing the LCDS locations calculated by different approaches. (b1–b4) Observed and simulated PSD versus L^* profiles from panels (a2–a5) averaged over four time intervals. Panels (b2–b4) correspond to the model results shown in (a3–a5), respectively. The green lines in (b2–b4) with hollow square symbols are copied from the data shown in panel (b1). (c1–c2) Blue and black curves: equatorial crossings of the electrons' trajectories from the test particle simulation for the LCDS from the TPR approach in blue, and TPI approach in black. The colors in the region with radial distances of 5–12 R_E represent the number of local magnetic field minima along the field lines: blue for one, green for two, red for at least three, and white region for open field lines. Panels (c1) and (c2) are plotted for the two times marked by the two red dashed vertical lines in (a1).

Initiated at MLT = 3, test particles are traced back to this MLT. Their northern mirror points over the traced drift shell are mapped to a sphere of 1 R_E radius to calculate the enclosed magnetic flux (Roederer & Zhang, 2014). This approach could more physically include the DOB effects than the second approach. The LCDS from this approach is the purple line in Figure 2a1, labeled LCDS(TPI). Due to the test particle simulation's computational intensity, we set the time resolution of both LCDS(TPR) and LCDS(TPI) at 10 min. The black line in Figure 2a1 is the rShue values. We find that if rShue were used as the approximation for LCDS, it could not lead to direct electron losses below $L^* = 6$ (Figure 2a2), since the minimum rShue value is greater than 6. Albert et al. (2018)

suggested that a shifted magnetopause, rShue – 2, may approximate the LCDS. However, for this event, rShue – 2 is around 4.2 at the end of interval #2, smaller than the other LCDS values across all Ks. Simulations using rShue – 2, which are not shown here, indicate an overestimation of electron loss at $L^* > 4.2$ during intervals #2, #3, and #4. Thus, neither rShue nor rShue – 2 serves as an effective LCDS proxy for this event. Comparatively, the LCDS values from the three different approaches in Figure 2a1 decrease to low L^* values during the storm main phase. Before 23 UT of May 27 and after 16 UT of May 28, LCDS(TPI) is generally the largest, LCDS(TPR) the smallest, and LCDS(TF) in between, aligning with Albert et al. (2018). This LCDS difference between the two test particle approaches could be understood using Figure 2c1, which is at 20 UT of May 27 marked by the first dashed vertical line in Figure 2a1. The colors in Figure 2c1 in the region with a radial distance of 5–12 R_E from Earth represent the number of local magnetic field minima along the local field line, with blue for one minimum, green for two minima, and red for at least three minima, respectively, while white color represents open field lines. We can see that the open field lines cover a wide region on the dayside due to the high solar wind P_{dyn} at this time. In addition, the high P_{dyn} compresses the dayside magnetosphere and leads to an increased local magnetic maximum at equator, which is favorable for DOB to occur. Consequently, a wide bifurcation region with two local magnetic field minima (green area) appears on the dayside, which leads to considerable differences between the LCDS(TPI) and LCDS(TPR) values as shown in Figure 2a1 at this time (marked by the first dashed vertical line). These two LCDS are also plotted in Figure 2c1 with TPR in blue and TPI in black. Specifically, these curves illustrate the equatorial crossings of the test electrons' trajectories at the LCDS. The gap in the black curve on the dayside is due to the bifurcated drift shells not crossing the equator. We can see that the LCDS(TPR) is located a lot closer to Earth than the LCDS(TPI), corresponding to the large difference between them.

However, between 23 UT of May 27 and 16 UT of May 28, the difference among the three LCDS values becomes much smaller. To understand this, in Figure 2c2 we create a similar magnetic configuration plot for the time of 00 UT on May 28 (marked by the second dashed vertical line in Figure 2a1). Lower solar wind P_{dyn} results in fewer open field lines (white) on the dayside and weaker magnetic fields in bifurcation maxima than Figure 2c1 shows. Additionally, a more southward IMF B_z causes a slimmer bifurcation region (green) due to enhanced reconnection. These factors cause smaller differences in LCDS values from the two test particle approaches, TPR (blue curve in Figure 2c2) and TPI (black curve). The gaps in both curves on the nightside result from the stretched asymmetric magnetic field lines with a complicated configuration. Furthermore, in Figure 2c2 we see a small red blob (with at least three local magnetic field minima) in the post-dusk region between 6 and 8 R_E, which is possibly related to a partial ring current on the nightside (Tsyganenko et al., 2021) but its physical cause and validity remain to be explored. This anomaly could cause unphysical open trajectories of electrons in between physical and closed drift shells of electrons. In our test particle approaches of calculating LCDS, we bypass this region for more physical LCDS values. From 23 UT of May 27 to 00 UT of May 28 (as shown in the zoomed-in plot on the right side of Figure 2a1), LCDS(TPR) remains the lowest, while LCDS(TF) is slightly higher than LCDS(TPI). This occurs when the tracing field lines approach can obtain an L^* value for a certain drift shell (by assuming constant second adiabatic invariant) while the test particle including DOB approach cannot since the particles are lost due to DOB.

3.2. Simulation Results in PSD

With the LCDS calculated by the three different approaches described above, we implement them into the radial diffusion model to quantify their effects on reproducing the observed electron losses. Figures 2a3–2a5 present the simulation results for the same μ and K values as the PSD data in Figure 2a2, with the white curves representing the LCDS values from the three different methods shown in Figure 2a1. Model 1 is with LCDS(TF), Model 2 is with LCDS(TPR), and Model 3 is with LCDS(TPI). We find that the models with different LCDS could all generate fast magnetopause shadowing loss of electrons at higher L^*, owing to the low LCDS values during the storm main phase. For detailed comparisons with data and examine the differences among the three approaches, we select four consecutive time intervals to investigate the detailed evolution of PSD versus L^* profiles. The time coverage for each interval is represented by a horizontal color bar above Figures 2a1–2a5. These intervals are: #1 (09 UT to 17 UT of May 27), #2 (17 UT to 23 UT of May 27), #3 (23 UT of May 27 to 00 UT of May 28), and #4 (00 UT to 09 UT of May 28). Figures 2b1–2b4 exhibit the comparison between data (Figure 2b1) and model results (Figures 2b2–2b4) in the evolution of PSD versus L^* profiles. We have assessed the uncertainty in the PSD values calculated from flux observations using the PSD matching method (Chen et al., 2005, 2007) following Reeves et al. (2013), and found an average uncertainty of a factor of 1.3 which is small. The profiles for intervals

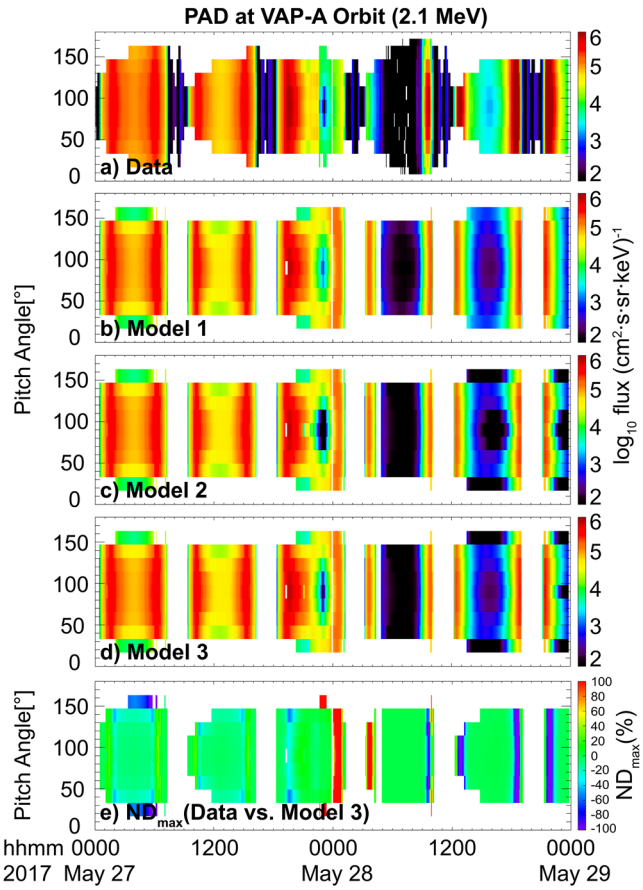

Figure 3. Observed (a) and modeled (b)–(d) PAD of electron fluxes at 2.1 MeV along Van Allen Probe A's orbit. Models 1–3 in panels (b)–(d) correspond to the different model settings depicted in Figure 2 (a3–a5). Panel (e) presents the normalized differences between observations and modeled flux from Model 3.

#1, #2, #3, and #4 are colored black, blue, green, and red, respectively. During interval #1, the pre-storm phase, both data and model exhibit similar profiles with positive PSD versus L^* gradient. During interval #2, the initial phase of the storm, LCDS(TPI) and LCDS (TF) stay higher than LCDS(TPR) (see Figure 2a1). By comparing the PSD versus L^* profiles during interval #2, we find that the data only show a very small drop at large L^* which is overestimated by Model 2 by rejecting field lines with DOB. This overestimation is improved in Model 1 and Model 3 which demonstrates that merely rejecting field lines with DOB in the LCDS calculation could lead to overestimation of the observed loss of electrons. The storm main phase is then divided into two intervals, intervals #3 and #4. During interval #3 as shown in the zoomed-in box of Figure 2a1, the LCDS(TF) stays the highest among the three, leading to a slight underestimation of the electron loss in Model 1 at high L^* regions compared to the data (marked by the green box in Figure 2b2). The green curve marked by the "+" symbols are model results, while the green curve marked by the hollow square symbols are PSD data copied from Figure 2b1. In contrast, the LCDS(TPR) reached as low as $L^* = 4.8$ at the beginning of this interval (orange curve in the zoomed-in plot of Figure 2a1) and remains low over most of the interval. Consequently, this causes an overestimation of the electron loss at high L^* regions during this interval by comparing the green curves inside the box in Figure 2b3. However, the LCDS(TPI) (purple in the zoomed-in plot) has a value generally in between LCDS(TF) and LCDS(TPR), which leads to a modeled PSD profile best matching the observations at high L^* regions (by comparing the green curves in the boxed region in Figure 2b4). These results show that physically including field lines with DOB in the LCDS calculation best captures the observed loss of electrons at high L^* regions. Finally for interval #4, by comparing the data and model results in Figures 2b1–2b4, we find that all three models well capture the observed electron dropout at high L^* regions. This is because the LCDS calculated by different approaches are close to each other during this interval as shown in Figure 2a1. By further looking at the PSD evolutions in all three models (Figures 2b2–2b4), we find the PSD profiles exhibit fast loss at large L^* and an internal PSD peak at low L^*, which are typical magnetopause shadowing loss features (Shprits et al., 2006; Turner et al., 2012).

3.3. Simulation Results in Flux

For a comprehensive comparison with data, we further convert the modeled PSD to electron flux in energy and pitch angle to directly compare with flux observations. Figure 3a presents the observed PAD of electron fluxes at 2.1 MeV along the orbit of Van Allen Probe A (identical to Figure 1c), and Figures 3b–3d display the modeled PAD of electron fluxes along the same orbit. The comparison shows that all models successfully reproduce the observed flux dropout between 5 and 9 UT of May 28 and the butterfly distribution near the apogee of Probe A around 23 UT of May 27, confirming the dominant effect of magnetopause shadowing loss in this dropout event at high L^*. Nevertheless, for the modeled butterfly PAD, Model 1 with LCDS(TF) underestimates the electron loss for pitch angles from approximately 65° to 115° (comparing Figures 3a–3b). Model 2 with LCDS(TPR), on the contrary, overestimates the electron loss at high pitch angles between ~65° and 115° (Figure 3c), while Model 3 with LCDS(TPI) exhibits the best agreement with the data. Moreover, to validate the modeled results against observations, we follow Wang et al. (2020) and calculate their difference normalized by the maximum average of the observed flux and simulated flux for each 8 hr (ND_{max}), which is shown in Figure 3e. The ND_{max} in Figure 3e indicates that Model 3 reproduces the observed flux well at high L^* and large pitch angles. Therefore, in addition to the modeled PSD results comparison, the PAD comparison in flux also demonstrates that modeling the magnetopause shadowing loss with the LCDS obtained by tracing particles and physically including DOB could better capture the electron loss at high L^* and outperforms the other two approaches. We note that all three models do not capture the observed electron loss at low L^* regions ($L^* < 4.8$ in Figures 2b1–2b4, red region in

Figure 3e), which could be due to other loss mechanisms such as the scattering by interactions with waves (e.g., EMIC waves). Additionally, the model underestimation after 12 UT on May 28 (blue regions in Figure 3e) may result from the lack of acceleration mechanisms in the model. Overall, our results show that Model 3 utilizing the LCDS obtained through tracing test particles and physically including DOB agrees the best with observations.

4. Conclusions and Discussion

During the May 2017 geomagnetic storm event, Van Allen Probes data show fast loss in electron PSD at large L^* across a wide range of μ values, and a butterfly pitch angle distribution in electron fluxes. These features highlight the significant role of magnetopause shadowing loss in the observed electron dropout. In this study, for the first time, we introduce an event-specific and K-dependent LCDS that physically includes the DOB effects, in comparison with two other LCDS that are less physical in addressing DOB, into a 1D radial diffusion model to quantitatively model the effects of DOB in the magnetopause shadowing loss of outer radiation belt electrons. Our major findings can be summarized below:

1. The fast dropout of outer radiation belt electrons at high L^* are dominated by magnetopause shadowing loss during this event. The shadowing loss is effectively reproduced by our radial diffusion model utilizing event-specific and K-dependent LCDS, suggesting that the inclusion of event-specific and K-dependent LCDS is crucial for accurately replicating the detailed features of magnetopause shadowing loss.
2. The differences among the calculated LCDS using the three approaches could vary depending on the geomagnetic conditions. During most of the storm, LCDS(TPR) (rejecting DOB) is smaller than LCDS(TF) (ignoring DOB), and both are smaller than LCDS(TPI) (physically including DOB). But for part of the storm main phase, the differences between the LCDS values become smaller.
3. By implementing the different LCDS into our radial diffusion model, we find that using LCDS(TF) underestimates the electron dropout during the initial storm main phase (interval #3) at high L^*, while using LCDS(TPR) overestimates the loss during that interval as well as the pre-storm interval (interval #2). However, using LCDS(TPI) that physically includes DOB well captures the shadowing loss during both the pre-storm and storm main phases and agrees the best with observations, in both the PSD versus L^* profiles and the flux pitch angle distributions.

Our results demonstrate the important role of DOB effects on the magnetopause shadowing loss of radiation belt electrons. Note that we have also tried using the LANLGeoMag (LGM) library (Henderson et al., 2018) to calculate the LCDS by tracing field lines with a constant second adiabatic invariant. Interestingly, the LCDS(TF) calculated using the LGM library is quite different from that using the IRBEM library. Instead, before the storm main phase, we find that LCDS(TF) using LGM mostly overlaps with the LCDS(TPR), which is consistent with the findings from Albert et al. (2018). Additionally, during the storm main phase, LCDS(TF) using LGM shows much lower values than those from the other methods shown in this paper, which is because the LCDS calculation using the LGM library often cannot bypass the region with the abnormal magnetic field lines illustrated in Figure 2c2 and discussed near the end of Section 3.1, leading to open drift shells at lower L^* values. These suggest that the filed line tracing approach assuming constant second adiabatic invariant does not work well with DOB, at least in the TS04 model for this event. Furthermore, there is still more future work to further improve the LCDS calculation and physically include the DOB effects. First, our results show that the DOB effects are dependent on the geomagnetic field conditions, thus their effects on magnetopause shadowing loss could vary among different storms. Future investigations examining various storms are necessary to better understand the effects of DOB on electron shadowing loss. Furthermore, it would be worthwhile to explore different magnetic models in the LCDS calculation such as the TS07 model (Tsyganenko & Sitnov, 2007) since the LCDS values can differ significantly among different field models (Albert et al., 2018). Finally, in this work we explore the DOB effects on the LCDS of electrons using a 1D radial diffusion model. To comprehensively include the electron transport due to DOB in both electron pitch angle and radial distance, a 3D diffusion model like DREAM3D (Tu et al., 2013) is needed and will be utilized in the future.

Data Availability Statement

The geomagnetic indices utilized in this study are obtained from OMNIWeb and can be accessed from https://cdaweb.gsfc.nasa.gov/. The data from the MagEIS and REPT instruments onboard Van Allen Probes can be obtained from https://rbsp-ect.newmexicoconsortium.org/science/DataDirectories.php. The model inputs and outputs used in this study are publicly available at Zenodo (Huang et al., 2023).

Acknowledgments
This work was supported by the NASA Grants 80NSSC19K0908, 80NSSC21K1312, and 80NSSC21K2008, DOE Grant DE-SC0020294, and NSF Grant AGS 1752736.

References

Albert, J. M., Selesnick, R. S., Morley, S. K., Henderson, M. G., & Kellerman, A. C. (2018). Calculation of last closed drift shells for the 2013 GEM radiation belt challenge events. *Journal of Geophysical Research: Space Physics*, *123*(11), 9597–9611. https://doi.org/10.1029/2018JA025991

Baker, D. N., Erickson, P. J., Fennell, J. F., Foster, J. C., Jaynes, A. N., & Verronen, P. T. (2018). Space weather effects in the Earth's radiation belts. *Space Science Reviews*, *214*(17), 17. https://doi.org/10.1007/s11214-017-0452-7

Baker, D. N., Kanekal, S. G., Hoxie, V. C., Batiste, S., Bolton, M., Li, X., et al. (2013). The relativistic electron-proton telescope (REPT) instrument on board the radiation belt storm probes (RBSP) spacecraft: Characterization of Earth's radiation belt high-energy particle populations. *Space Science Reviews*, *179*(1–4), 337–381. https://doi.org/10.1007/s11214-012-9950-9

Blake, J. B., Carranza, P. A., Claudepierre, S. G., Clemmons, J. H., Crain, W. R., Dotan, Y., et al. (2013). The magnetic electron ion spectrometer (MagEIS) instruments aboard the radiation belt storm probes (RBSP) spacecraft. *Space Science Reviews*, *179*(1–4), 383–421. https://doi.org/10.1007/s11214-013-9991-8

Blum, L. W., Halford, A., Millan, R., Bonnell, J. W., Goldstein, J., Usanova, M., et al. (2015). Observations of coincident EMIC wave activity and duskside energetic electron precipitation on 18–19 January 2013. *Geophysical Research Letters*, *42*(14), 5727–5735. https://doi.org/10.1002/2015GL065245

Boscher, D., Bourdarie, S., O'Brien, P., Guild, T., Heynderickx, D., Morley, S., et al. (2022). PRBEM/IRBEM: v5.0.0. *Zenodo*. https://doi.org/10.5281/zenodo.6867552

Brautigam, D. H., & Albert, J. M. (2000). Radial diffusion analysis of outer radiation belt electrons during the October 9, 1990, magnetic storm. *Journal of Geophysical Research*, *105*(A1), 291–309. https://doi.org/10.1029/1999ja900344

Brizard, A. J., & Chan, A. A. (1999). Nonlinear relativistic gyrokinetic Vlasov-Maxwell equations. *Physics of Plasmas*, *6*(12), 4548–4558. https://doi.org/10.1063/1.873742

Capannolo, L., Li, W., Ma, Q., Shen, X.-C., Zhang, X.-J., Redmon, R. J., et al. (2019). Energetic electron precipitation: Multievent analysis of its spatial extent during EMIC wave activity. *Journal of Geophysical Research: Space Physics*, *124*(4), 2466–2483. https://doi.org/10.1029/2018JA026291

Chen, Y., Friedel, R. H. W., Reeves, G. D., Cayton, T. E., & Christensen, R. (2007). Multisatellite determination of the relativistic electron phase space density at geosynchronous orbit: An integrated investigation during geomagnetic storm times. *Journal of Geophysical Research*, *112*(A11), A11214. https://doi.org/10.1029/2007ja012314

Chen, Y., Friedel, R. H. W., Reeves, G. D., Onsager, T. G., & Thomsen, M. F. (2005). Multisatellite determination of the relativistic electron phase space density at geosynchronous orbit: Methodology and results during geomagnetically quiet times. *Journal of Geophysical Research*, *110*(A10), A10210. https://doi.org/10.1029/2004JA010895

George, H., Reeves, G., Cunningham, G., Kalliokoski, M. M. H., Kilpua, E., Osmane, A., et al. (2022). Contributions to loss across the magnetopause during an electron dropout event. *Journal of Geophysical Research: Space Physics*, *127*(10), e2022JA030751. https://doi.org/10.1029/2022JA030751

Henderson, M., Morley, S., Niehof, J., & Larsen, B. (2018). drsteve/LANLGeoMag v1.5.16. https://doi.org/10.5281/zenodo.1195041

Huang, J., Lyu, X., Tu, W., Albert, J. M., & Lee, S.-Y. (2023). Modeling the effects of drift orbit bifurcation on the magnetopause shadowing loss of radiation belt electrons [Dataset]. Zenodo. https://doi.org/10.5281/zenodo.8336642

Huang, J., Tu, W., & Eshetu, W. W. (2022). Modeling the effects of drift orbit bifurcation on radiation belt electrons. *Journal of Geophysical Research: Space Physics*, *127*(11), e2022JA030827. https://doi.org/10.1029/2022JA030827

Katsavrias, C., Daglis, I. A., & Li, W. (2019). On the statistics of acceleration and loss of relativistic electrons in the outer radiation belt: A superposed epoch analysis. *Journal of Geophysical Research: Space Physics*, *124*(4), 2755–2768. https://doi.org/10.1029/2019JA026569

Li, W., Ma, Q., Thorne, R. M., Bortnik, J., Zhang, X. J., Li, J., et al. (2016). Radiation belt electron acceleration during the 17 March 2015 geomagnetic storm: Observations and simulations. *Journal of Geophysical Research: Space Physics*, *121*(6), 5520–5536. https://doi.org/10.1002/2016JA022400

Lyu, X., Ma, Q., Tu, W., Li, W., & Capannolo, L. (2022). Modeling the simultaneous dropout of energetic electrons and protons by EMIC wave scattering. *Geophysical Research Letters*, *49*(20), e2022GL101041. https://doi.org/10.1029/2022GL101041

Miyoshi, Y., Jordanova, V. K., Morioka, A., Thomsen, M. F., Reeves, G. D., Evans, D. S., & Green, J. C. (2006). Observations and modeling of energetic electron dynamics during the October 2001 storm. *Journal of Geophysical Research*, *111*(A11), A11S02. https://doi.org/10.1029/2005JA011351

Olifer, L., Mann, I. R., Morley, S. K., Ozeke, L. G., & Choi, D. (2018). On the role of last closed drift shell dynamics in driving fast losses and Van Allen radiation belt extinction. *Journal of Geophysical Research: Space Physics*, *123*(5), 3692–3703. https://doi.org/10.1029/2018JA025190

Olifer, L., Mann, I. R., Ozeke, L. G., Claudepierre, S. G., Baker, D. N., & Spence, H. E. (2021). On the similarity and repeatability of fast radiation belt loss: Role of the last closed drift shell. *Journal of Geophysical Research: Space Physics*, *126*(11), e2021JA029957. https://doi.org/10.1029/2021JA029957

Öztürk, M. K., & Wolf, R. A. (2007). Bifurcation of drift shells near the dayside magnetopause. *Journal of Geophysical Research*, *112*(A7), A07207. https://doi.org/10.1029/2006JA012102

Reeves, G. D., Spence, H. E., Henderson, M. G., Morley, S. K., Friedel, R. H. W., Funsten, H. O., et al. (2013). Electron acceleration in the heart of the Van Allen radiation belts. *Science*, *341*(6149), 991–994. https://doi.org/10.1126/science.1237743

Roederer, J. G., & Zhang, H. (2014). *Dynamics of magnetically trapped particles: Foundations of the physics of radiation belts and space plasmas*. Astrophysics and Space Science Library, Springer. https://doi.org/10.1007/978-3-642-41530-2

Sarris, T. E., Li, X., Zhao, H., Papadakis, K., Liu, W., Tu, W., et al. (2022). Distribution of ULF wave power in magnetic latitude and local time using THEMIS and Arase measurements. *Journal of Geophysical Research: Space Physics*, *127*(10), e2022JA030469. https://doi.org/10.1029/2022JA030469

Schulz, M., & Lanzerotti, L. (1974). *Particle diffusion in the radiation belts*. Springer.

Shprits, Y. Y., Daae, M., & Ni, B. (2012). Statistical analysis of phase space density buildups and dropouts. *Journal of Geophysical Research*, *117*(A1), A01219. https://doi.org/10.1029/2011JA016939

Shprits, Y. Y., Drozdov, A. Y., Spasojevic, M., Kellerman, A. C., Usanova, M. E., Engebretson, M. J., et al. (2016). Wave-induced loss of ultra-relativistic electrons in the Van Allen radiation belts. *Nature Communications*, *7*(1), 12883. https://doi.org/10.1038/ncomms12883

Shprits, Y. Y., Thorne, R. M., Friedel, R., Reeves, G. D., Fennell, J., Baker, D. N., & Kanekal, S. G. (2006). Outward radial diffusion driven by losses at magnetopause. *Journal of Geophysical Research*, *111*(A11), A11214. https://doi.org/10.1029/2006JA011657

Shue, J. H., Song, P., Russell, C. T., Steinberg, J. T., Chao, J. K., Zastenker, G., et al. (1998). Magnetopause location under extreme solar wind conditions. *Journal of Geophysical Research*, *103*(A8), 17691–17700. https://doi.org/10.1029/98JA01103

Tsyganenko, N. A., Andreeva, V. A., & Sitnov, M. I. (2021). Reconstruction of magnetospheric storm-time dynamics using cylindrical basis functions and multi-mission data mining. *Journal of Geophysical Research: Space Physics*, *126*(2), e2020JA028390. https://doi.org/10.1029/2020JA028390

Tsyganenko, N. A., & Sitnov, M. I. (2005). Modeling the dynamics of the inner magnetosphere during strong geomagnetic storms. *Journal of Geophysical Research*, *110*(A3), A03208. https://doi.org/10.1029/2004JA010798

Tsyganenko, N. A., & Sitnov, M. I. (2007). Magnetospheric configurations from a high-resolution data-based magnetic field model. *Journal of Geophysical Research*, *112*(A6), A06225. https://doi.org/10.1029/2007JA012260

Tu, W., Cunningham, G. S., Chen, Y., Henderson, M. G., Camporeale, E., & Reeves, G. D. (2013). Modeling radiation belt electron dynamics during GEM challenge intervals with the DREAM3D diffusion model. *Journal of Geophysical Research: Space Physics*, *118*(10), 6197–6211. https://doi.org/10.1002/jgra.50560

Tu, W., Cunningham, G. S., Chen, Y., Morley, S. K., Reeves, G. D., Blake, J. B., et al. (2014). Event-specific chorus wave and electron seed population models in DREAM3D using the Van Allen Probes. *Geophysical Research Letters*, *41*(5), 1359–1366. https://doi.org/10.1002/2013GL058819

Tu, W., Li, X., Chen, Y., Reeves, G. D., & Temerin, M. (2009). Storm-dependent radiation belt electron dynamics. *Journal of Geophysical Research*, *114*(A2), A02217. https://doi.org/10.1029/2008JA013480

Tu, W., Selesnick, R., Li, X., & Looper, M. (2010). Quantification of the precipitation loss of radiation belt electrons observed by SAMPEX. *Journal of Geophysical Research*, *115*(A7), A07210. https://doi.org/10.1029/2009JA014949

Tu, W., Xiang, Z., & Morley, S. K. (2019). Modeling the magnetopause shadowing loss during the June 2015 dropout event. *Geophysical Research Letters*, *46*(16), 9388–9396. https://doi.org/10.1029/2019GL084419

Turner, D. L., Angelopoulos, V., Morley, S. K., Henderson, M. G., Reeves, G. D., Li, W., et al. (2014). On the cause and extent of outer radiation belt losses during the 30 September 2012 dropout event. *Journal of Geophysical Research: Space Physics*, *119*(3), 1530–1540. https://doi.org/10.1002/2013JA019446

Turner, D. L., Shprits, Y., Hartinger, M., & Angelopoulos, V. (2012). Explaining sudden losses of outer radiation belt electrons during geomagnetic storms. *Nature Physics*, *8*(3), 208–212. https://doi.org/10.1038/nphys2185

Ukhorskiy, A. Y., Anderson, B. J., Brandt, P. C., & Tsyganenko, N. A. (2006). Storm time evolution of the outer radiation belt: Transport and losses. *Journal of Geophysical Research*, *111*(A11), A11S03. https://doi.org/10.1029/2006JA011690

Ukhorskiy, A. Y., Sitnov, M. I., Millan, R. M., & Kress, B. T. (2011). The role of drift orbit bifurcations in energization and loss of electrons in the outer radiation belt. *Journal of Geophysical Research*, *116*(A9), A09208. https://doi.org/10.1029/2011JA016623

Ukhorskiy, A. Y., Sitnov, M. I., Millan, R. M., Kress, B. T., & Smith, D. C. (2014). Enhanced radial transport and energization of radiation belt electrons due to drift orbit bifurcations. *Journal of Geophysical Research: Space Physics*, *119*(1), 163–170. https://doi.org/10.1002/2013JA019315

Van Allen, J. A., Ludwig, G. H., Ray, E. C., & McIlwain, C. E. (1958). Observation of high intensity radiation by satellites 1958 alpha and gamma. *Jet Propulsion*, *28*(9), 588–592. https://doi.org/10.2514/8.7396

Van Allen, J. A., McIlwain, C. E., & Ludwig, G. H. (1959). Satellite observations of electrons artificially injected into the geomagnetic field. *Journal of Geophysical Research*, *64*(8), 877–891. https://doi.org/10.1029/JZ064i008p00877

Wang, D., & Shprits, Y. Y. (2019). On how high-latitude chorus waves tip the balance between acceleration and loss of relativistic electrons. *Geophysical Research Letters*, *46*(14), 7945–7954. https://doi.org/10.1029/2019GL082681

Wang, D., Shprits, Y. Y., Zhelavskaya, I. S., Effenberger, F., Castillo, A., Drozdov, A. Y., et al. (2020). The effect of plasma boundaries on the dynamic evolution of relativistic radiation belt electrons. *Journal of Geophysical Research: Space Physics*, *125*(5), e2019JA027422. https://doi.org/10.1029/2019JA027422

Xiang, Z., Tu, W., Li, X., Ni, B., Morley, S. K., & Baker, D. N. (2017). Understanding the mechanisms of radiation belt dropouts observed by Van Allen Probes. *Journal of Geophysical Research: Space Physics*, *122*(10), 9858–9879. https://doi.org/10.1002/2017JA024487

Xiang, Z., Tu, W., Ni, B., Henderson, M. G., & Cao, X. (2018). A statistical survey of radiation belt dropouts observed by Van Allen Probes. *Geophysical Research Letters*, *45*(16), 8035–8043. https://doi.org/10.1029/2018GL078907

Yu, Y., Koller, J., & Morley, S. K. (2013). Quantifying the effect of magnetopause shadowing on electron radiation belt dropouts. *Annales Geophysicae*, *31*(11), 1929–1939. https://doi.org/10.5194/angeo-31-1929-2013

Zhang, X.-J., Li, W., Ma, Q., Thorne, R. M., Angelopoulos, V., Bortnik, J., et al. (2016). Direct evidence for EMIC wave scattering of relativistic electrons in space. *Journal of Geophysical Research: Space Physics*, *121*(7), 6620–6631. https://doi.org/10.1002/2016JA022521